



# An assessment of the contact rates between individuals when movement is modelled by a correlated random walk

Joseph D. Bailey<sup>1</sup>

Received: 27 March 2022 / Accepted: 12 July 2023  
© The Author(s) 2023

## Abstract

Understanding how individuals come into contact with each other is important in many fields from biology and ecology to robotics and physics. Interaction dynamics are central in understanding how information is spread between agents, how disease spreads through a population, and how group movement or behaviour occurs. However, in many applications, the underlying mode of movement is not considered, and instead, contacts are considered a fraction of all possible contacts amongst a population. This gives rise to the mass-action law which in turn implies a negative quadratic relationship between contacts and individuals. Here we consider how a simple but often used movement model, the correlated random walk, affects the contact rate in a standard Susceptible-Infection (SI) epidemiological model. Via extensive simulation, we show that the contact rate is not always well described by the assumed negative quadratic relationship,  $I(N - I)$  (where  $I$  is the number of infected at a given time and  $N$  the total number of individuals). Instead, we find that a contact rate proportional to  $[I(N - I)]^\alpha$  with  $0 < \alpha \leq 1$  is a better qualitative fit, where  $\alpha$  depends upon parameters such as the straightness of the movement and the density of individuals. We highlight that the expected contacts at low densities increase with straight line movement, whereas, at high densities, they increase with more random movement.

**Keywords** Contact rate · Animal movement · Correlated random walk · Disease spread · Information spread

## Introduction

The way in which individuals move in an environment can have a profound effect on interaction dynamics, such as the number and frequency of contacts between individuals (Fofana and Hurford 2017; White et al. 2018). This information is important for exploring group level phenomena including group behaviour, information exchange and disease spread. Understanding interaction dynamics has important ramifications and uses in a variety of fields, from movement strategies in robotics (Goldberg and Matarić 1999; Pang et al. 2021) and information spread in the social sciences (Huang 2000; Zhou et al. 2020) to epidemiology (Fofana and Hurford 2017; White et al. 2018) and particle dynamics (Liggett 2012; Jiao and Gonella 2020). Currently, most mathematical models of these processes do not consider the specific movement modes of individuals, averaging

out the movement patterns across spatial scales and environments. Such averaging of movement at the population level is known to cause significant differences in predicted and observed behaviour (Franz and Erban 2013) and can miss important dynamics which are apparent when considering local or individual behaviour (Tang and Bennett 2010).

Movement ecology is the established field concerned with understanding and predicting the spatial characteristics of movement at both individual and group level, from local small-scale movement to long range relocations between countries and continents (Nathan et al. 2008). Incorporating movement ecology into models of interaction dynamics by explicitly including models of predicted movement will lead to more realistic descriptions of processes such as information or disease spread. Whilst there have been attempts to more closely integrate the fields of movement ecology and epidemiology (Tracey et al. 2014; Fofana and Hurford 2017; Dougherty et al. 2018; White et al. 2018), there are still many unanswered important questions regarding interaction dynamics, specifically, determining the precise relationship between the number of individuals and the expected number of interactions, and how this relates to different models of

✉ Joseph D. Bailey  
jbailef@essex.ac.uk

<sup>1</sup> Department of Mathematical Sciences, University of Essex, Colchester, Essex CO4 3SQ, UK

movement and spatial behaviours (Fofana and Hurford 2017; White et al. 2018).

Movement is a complex process reliant on many internal and external stimuli (Nathan et al. 2008). However, simple models are often used in analysing, predicting, and understanding movement behaviour, including diffusion processes (Blackwell 1997; Ovaskainen 2004), Brownian motion (Horne et al. 2007; de Jager et al. 2014; Bearup et al. 2016), agent-based models (Tang and Bennett 2010; McDermott et al. 2017), and both continuous and discrete random walks (Codling et al. 2008; Johnson et al. 2008; Bailey et al. 2018). Discrete random walks are commonly used in the field of movement ecology (Kareiva and Shigesada 1983; Codling et al. 2008) due to their relative simplicity and the nature of telemetry data being recorded as a discrete-time series. Random walk theory has been used to describe and analyse the behaviour of a wide range of animals, from the small and micro-scale movements of cells (Codling et al. 2008; Li et al. 2010), bacteria (Theves et al. 2015), and insects (Kareiva and Shigesada 1983; Bailey et al. 2021a) to the large and macro-displacements of elk (Fortin et al. 2005), whales (Whitehead et al. 2008), and seabirds (Bartumeus et al. 2010). As well as across time scales, from high frequency multiple locations per second for short scale fast movement (Bailey et al. 2021b), to sparse daily or monthly data when monitoring large scale movement of migrations (Bergman et al. 2000).

When modelling movement by a discrete random walk (RW) at the individual level, the most common approaches are to use the following: a simple random walk (SRW), in which the direction of each step is taken at random, giving rise to movement closely linked with Brownian motion; a biased random walk (BRW), in which there is a preference for a specific direction at each timestep, this could be either towards a global compass direction or towards a specific location in space; or a correlated random walk (CRW), in which the movement direction at each time step is governed by the direction of movement at the previous time step (termed persistence), leading to a movement path which has a localised or short term bias in direction (Codling et al. 2008). However, this local bias disappears as the number of time steps increase and the CRW in the long run mimics a SRW; the speed of this convergence is dependent upon the strength of correlation in successive steps, with weakly correlated movement mimicking a SRW faster (Benhamou 2006). This correlation in movement results in the CRW exhibiting non-Markov behaviour as each step is dependent upon the previous step of the process.

As discussed in Fofana and Hurford (2017), a central assumption in many traditional formulations of contact rates between individuals in a large population is that of homogenous mixing and instantaneous contact. That is, each individual is as likely to come into contact with every single

other individual within the population at any given time point. This gives rise to the ‘mass-action’ law, describing a negative quadratic relationship that governs the number of expected contacts. This approximation has successfully been used in many epidemiology models and is used to determine important parameters in disease spread, such as the reproductive number  $R_0$ . However, by including more specific rules regarding the movement of individuals, the assumptions that give rise to the mass-action law may be violated.

Whilst other models do more directly consider contact rates via data analysis (Otten et al. 2003; Richomme et al. 2006; Hudson et al. 2019), network theory and analysis (Bansal et al. 2007; 2010; Volkova et al. 2010) or via extensive simulations (Kirkeby et al. 2017; Hudson et al. 2019), these are usually post hoc and rely on recorded or observed data to become available and subsequently analysed. Fofana and Hurford (2017) considered how simple random walk models can influence contact rates, indicating that when included in a simple Susceptible-Infection (SI) model the mass-action law was still appropriate, with a CRW, BRW, and Lévy Walk giving qualitatively similar results. However, here by more extensive simulations, we demonstrate that this contact rate does not strictly follow the predicted negative quadratic relationship for a CRW, instead, more closely following  $[I(N - I)]^\alpha$  with  $0 < \alpha \leq 1$ , where  $I$  is the number of infected at a given time and  $N$  the total number of individuals. We demonstrate that the density of individuals has a large impact on this value of  $\alpha$ .

## Methods

### Justification for use of a CRW

Although the drivers of movement are incredibly complex, requiring inputs from internal factors as well as reactions to both the environment and the movement of other individuals, CRWs have been used extensively as proxies to animal movement, in order both to analyse observed data and to describe movement in theoretical models. Whilst it is clear CRW are limited in their accuracy at recreating realistic animal movement (Fagan and Calabrese 2014), the model is still widely used, especially with ‘simpler’ organisms such as plankton (Menden-Deuer 2010), microalga *Chlamydomonas reinhardtii* (Garcia et al. 2011), and insects (Kareiva and Shigesada 1983; Gui et al. 2012; Loureiro and Nams 2020). Recently, CRW have found applications in the movement of robotics, becoming a popular choice of movement model when working with swarm robotics, to programme efficient area search algorithms (Dimidov et al. 2016; Pang et al. 2019, 2021; Renzaglia and Briñón-Arranz 2020) and exploration mapping (Kegeleirs et al. 2019). CRWs are also used in the current theoretical work on the movement of

groups of insects confined to experimental arenas, to determine the optimal network of traps (Manoukis et al. 2014; Bau and Cardé, 2016), the most efficient shape and size of insect traps (Ahmed and Petrovskii 2019), understand general movement of insects (Byers 2009; Wittman et al. 2019), encounter rates (Byers and Naranjo 2014), as well as to describe the population diffusion and invasive capabilities of a species (Turchin 1998) which in turn help inform IPM strategies (Allema et al. 2010; Banks et al. 2020). CRWs have also been shown to consider more complex group level behaviour when multiple CRWs are combined (Haydon et al. 2008). Due to CRWs often being seen as a null model for simple movement (Fagan and Calabrese 2014), they are prevalent when attempting to understand or predict phenomena which require underlying movement. For example, when analysing landscape connectivity and its relationship with invasive insects (Koh et al. 2013), modelling invasive spread of plants (Andersen et al. 2005) is frequently still used as a base model when attempting to classify movement (Reynolds et al. 2013; Grant et al. 2018; Bailey et al. 2021a), with examples of CRW being observed in various animals, such as insects including Colorado potato beetles (Gui et al. 2012), moths (Bau and Cardé 2016), bark beetles (Byers 2001), and *Harpalus rufipes* beetles (Loureiro and Nams 2020) along with larger animals such as manta ray when foraging (Papastamatiou et al. 2012), elk (Fortin et al. 2005), and Cory's shearwater sea birds (Focardi and Cecere 2014).

## Details of model and simulation

In this work, we will use the general terminology of epidemiology and consider a population consisting of individuals who are either infected or susceptible. This is for clarity and to be in keeping with previous similar work, but the results are not intended to focus solely on that field. For example, an infected individual can be thought of as an agent who has information, and a susceptible individual is equivalent to an agent who has yet to receive the information.

To determine the number of contacts between infected and susceptible individuals given as a function of the number of infected, we consider a fixed population of size  $N$ , with each individual moving determined by a CRW in a confined square arena with length,  $L$ , and a reflective boundary (Bearup and Petrovskii 2015). A reflective boundary was chosen to prevent large groups collecting at the boundary (see Supplementary Material File 1), and as the model is aimed at recreating movement in a restricted area, a periodic boundary was not considered. The precise geometry of the arena and laws governing the border can have an effect on movement behaviour (such as for trap efficiency (Ahmed and Petrovskii 2019) and in the analysis of persistence in movement (Christensen et al. 2021)); however, these are not

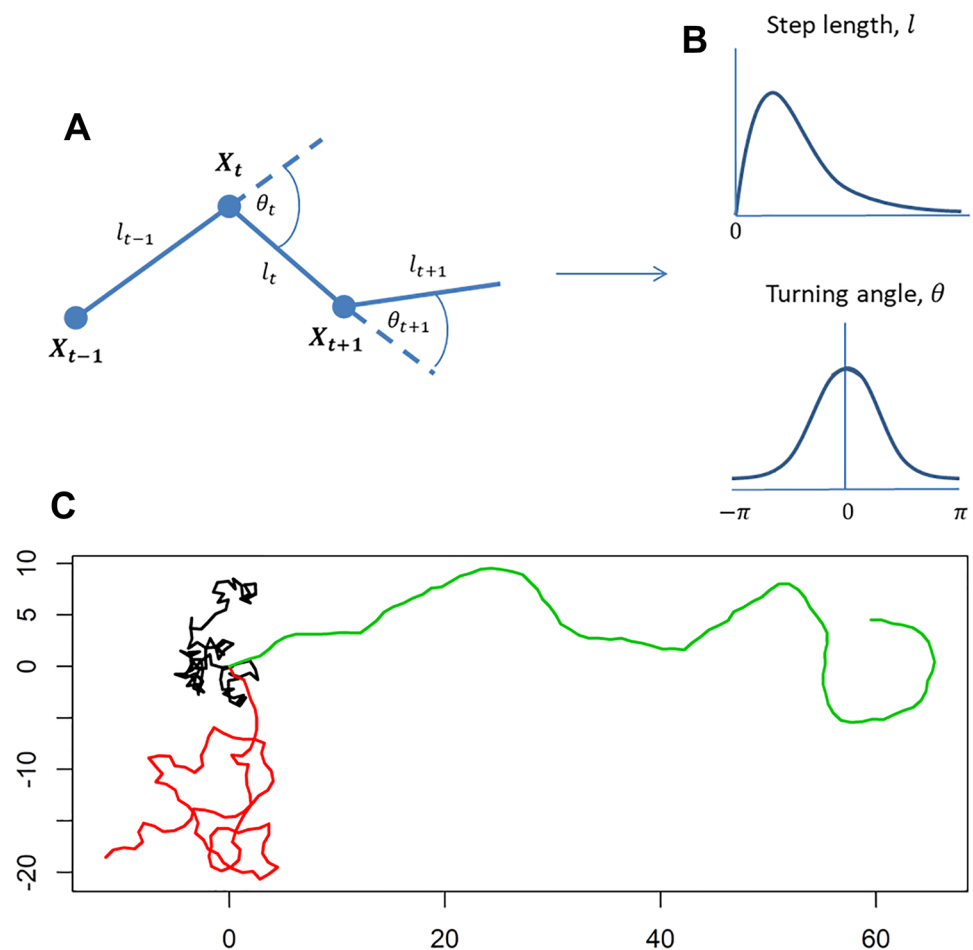
investigated here. The population is initially randomly uniformly placed within the arena.

We only consider a binary state space for each individual in which each is either infected or susceptible. With the infected state acting as an absorbing state, that is, when an agent becomes infected, they remain infected for the duration, can continue to pass on the infection, and cannot leave the population—this is equivalent to the simple Susceptible-Infection (SI) model in epidemiology. Each simulation begins with one randomly located infected individual and continues until the entire population is infected. We denote the number of infected by  $I$  and the number of susceptible by  $S$  (giving the standard relationship of  $N = S + I$ ).

We define the contact distance,  $r$ , as the distance below which a contact is considered to be made. This value was taken as 0.5, 1, and 2, with  $r = 2$  used unless stated otherwise. As the model uses a discrete time random walk, a contact can only be considered to be made at the end of each step (at each  $X_t$  in Fig. 1) and not anywhere between successive steps. The probability of a successful contact,  $p_{SI}$ , that is a contact in which infection is successfully passed, is explored using four simple rules: (i)  $p_{SI} = 1$ ; (ii)  $p_{SI} = 0.5$ ; (iii)  $p_{SI} = r - d_{SI}$ , (with  $p_{SI} = 0$  if  $d_{SI} \geq r$ ) where  $d_{SI}$  is the distance between the susceptible and infected individuals giving a linear relationship between distance and a successful contact; and (iv)  $p_{SI} = 1/(1 + d_{SI})^2$  (with  $p_{SI} = 0$  if  $d_{SI} \geq r$ ) giving an inverse square relationship between distance and a successful contact. Unless stated otherwise, the main text focuses on the simplest case,  $p_{SI} = 1$ . As a contact is not considered to be a physical interaction, individuals continue moving in the same manner after a contact as they were before the contact, similar to other studies (Fofana and Hurford 2017; Ahmed et al. 2021).

2d discrete-time continuous-space CRWs are determined by the distance between locations (step lengths) and turning angles (difference in directions between successive locations) (Kareiva and Shigesada 1983) (Fig. 1). It should be noted that whilst the precise form of these underlying distributions is known to have an effect on the resulting movement path (Bartumeus et al. 2008; Codling et al. 2010), as we are interested in contact rates across groups moving with the same movement parametrisations, the quantitative differences should be minimal. However, in order to control for this, we considered step lengths drawn from three distributions: a Rayleigh distribution (with scale parameter  $\sigma = 1$ ), a uniform distribution, and a fixed distance (fixed at either 1 or 2 units—note, unless otherwise stated the fixed distance of length 1 unit was used throughout). Turning angles were drawn from one of two distributions: a uniform or a wrapped normal. To investigate how the straightness of the movement path effected the results, the concentration parameter,  $\rho$ , of the wrapped normal distribution took values of 0.5, 0.7, 0.9, 0.95, and 0.99. Lower values correspond to more winding

**Fig. 1** **A** Example of a discrete RW described by locations  $X_{t-1}, X_t, X_{t+1}$ , with distance between locations (step-lengths) given by  $l_{t-1}, l_t, l_{t+1}$  and difference in direction of movement (turning angles) given as  $\theta_t, \theta_{t+1}$ . The step-lengths and turning angles can be modelled by or drawn from probability functions. **B** In the case for a CRW, the turning angle distribution would be centred around 0 (mean=0). **C** gives examples of three CRWs each with constant step length (1 unit) and turning angles drawn from a zero centred wrapped normal distribution; however, each has a different value for the concentration parameter,  $\rho$ , of the wrapped normal distribution:  $\rho = 0$  (black)—corresponding to random movement;  $\rho = 0.7$  (red);  $\rho = 0.95$  (green). Note the higher the value for  $\rho$  the straighter the movement



movement (closer to a SRW) and values closer to 1 give straighter movement (note the use of a uniform distribution is equivalent to setting  $\rho = 0$  in a wrapped normal distribution) (Fig. 1). These specific distributions and parameter values were chosen as they are similar to those used in previous, comparable general movement studies (Fofana and Hurford 2017; Bailey et al. 2018; Ahmed and Petrovskii 2019; Bailey and Codling 2021).

Simulations were run with a fixed arena size of  $50 \times 50$  units featuring a population of  $N = 50, 250, 1000$  and  $2500$  giving relative densities of  $D = 0.02, 0.1, 0.4$  and  $1$  agents per unit squared. These values are also similar to those found in comparative studies (Fofana and Hurford 2017).

All parameters are detailed in Table 1. Results were averaged over 10,000 simulations, with all calculations carried out in R (R Core Team 2020).

### Analytical predictions

In the case for a uniform distribution of step lengths, the number of contacts given  $I$  infected individuals is equivalent to the proportion of the arena expected to be covered by  $I$

circles of radius  $r$ . This is due to the model at each time point essentially randomly placing all individuals within the arena. This can be precisely formulated in the case where the boundary is periodic (that is movement is considered to be on a torus) (Hall 1988). Note this is the case for any type of turning angle distribution and contact distance.

### Results

In general, it is clear that the negative quadratic given by the assumed mass-action law is not a good universal fit for the results, whereas the modified expression of  $[I(N - I)]^\alpha$  gives a quantitatively better fit. The results of the simulations when using a constant step length of 1 unit and a contact radius of  $r = 2$  units, with the infection being passed on with certainty given a contact ( $p_{SI} = 1$ ), are shown in Fig. 2. In all panels, the solid curves correspond to differing values of the concentration parameter of the wrapped normal distribution,  $\rho$ , taking values of 0, 0.5, 0.7, 0.9, 0.95, and 0.99, going from dark to light respectively (recalling that values close to

**Table 1** Detailing the parameters and values used for the simulations

Parameter	Description	Values
$N$	Total number of individuals	50, 250, 1000, 2500
$L$	Length of sides of simulation arena	50 units
$D$	Density of individuals ( $N/L^2$ )	0.02, 0.1, 0.4, 1 individuals per sq. unit
$\rho$	Concentration parameter of wrapped normal distribution for the turning angle	0, 0.5, 0.7, 0.9, 0.95, 0.99
$sl$	Step-length distribution	- Fixed length: 1, 2 units - Rayleigh Distribution ( $\sigma = 1$ ) - Uniform Distribution
$r$	Contact distance (distance at which two individuals are deemed in contact)	0.5, 1, 2 units
$p_{SI}$	Probability of a successful contact given a susceptible and an Infected individual are within contact distance	$p_{SI} = 1$ $p_{SI} = 0.5$ $p_{SI} = r - d_{SI}$ $p_{SI} = 1/(1 + d_{SI})^2$ (where $p_{SI} = 0$ whenever $d_{SI} \geq r$ )

0 give more random movement, and values close to 1 give straighter movement).

Focusing on how the density effects the results, we see that for relatively high densities the negative quadratic of the mass-action law is a good fit to the simulated results, but this goodness of fit is lost with decreasing densities, with the negative quadratic failing to demonstrate important features of the simulated results. Noticeably, as the density increases, the more similar the curves and at  $D = 1$  the results are near indistinguishable. The best fitting negative quadratic curves, as predicted by mass-action, are shown in Fig. 2 by the blue dotted lines (Fig. 2a, c, e, g). For  $D > 0.02$ , the simulations exhibit flatter peaks, steeper sides, and a negative skewness compared with the best fitting negative quadratic. In all cases, for low or high numbers of Infected, the contact rate is higher than the predicted quadratic curve, often by orders of magnitude of 2–5. However, if we compare the results with a predicted growth of order  $[I(N - I)]^\alpha$  (Fig. 2b, d, f, h—red dashed), we note that the characteristics of the predicted curve more closely match the results, especially as the density increases.

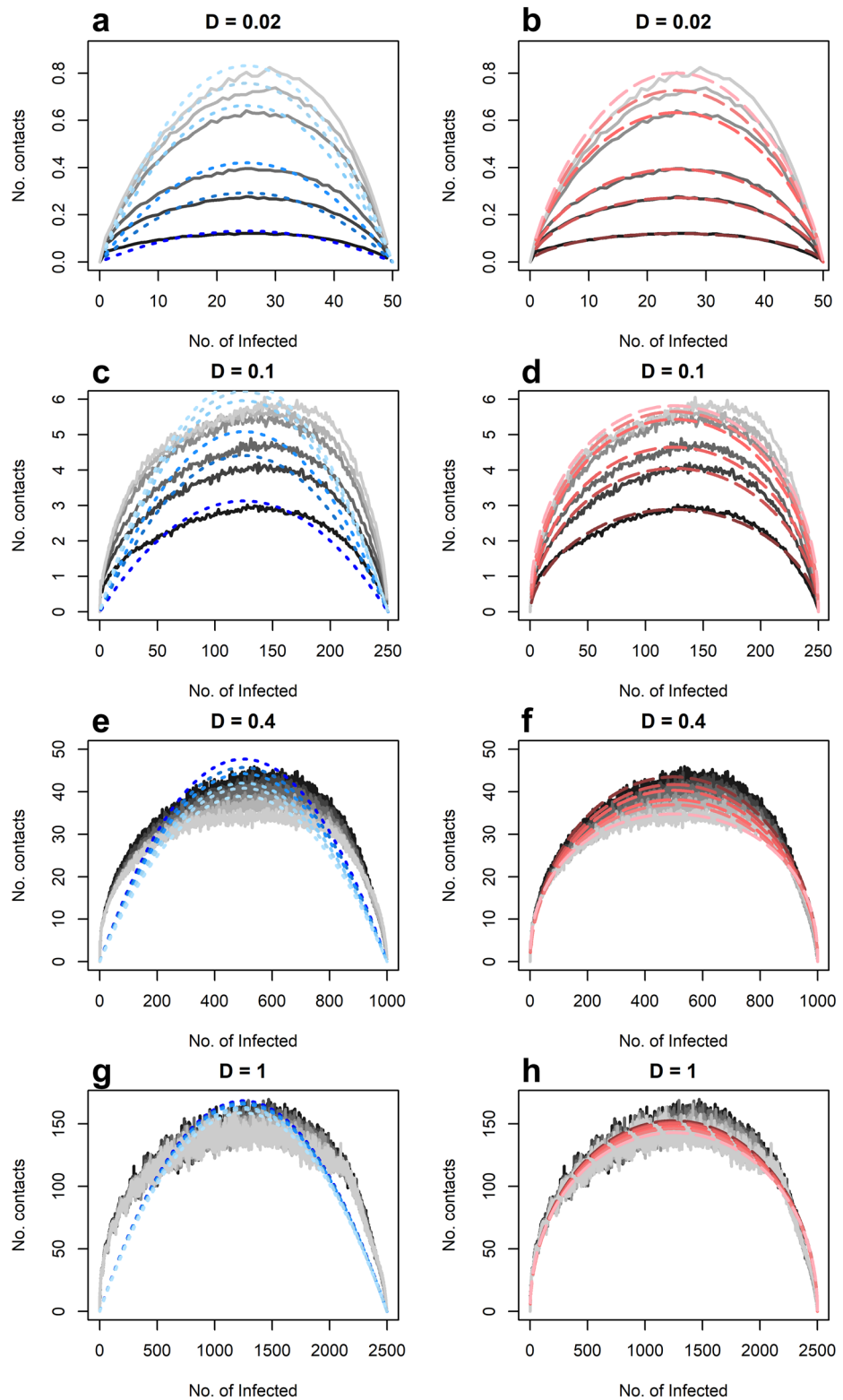
It is clear, however, that none of the predicted curves accurately reflect the skewedness in the simulated results. Although this can be explained by considering that, after a few timesteps with  $k$  infected, we would expect all  $k$  infected individuals to be close to each other (due to the movement model) and their ‘reach’ for contacting susceptible individuals to be governed by the length of the perimeter of the shape that covers them. If we now consider precisely  $k$  susceptible individuals (equivalent to  $N - k$  infected), we expect them to be spread around the arena and not clustered together in one group, as was the case for when there were  $k$  infected. Therefore, the length of the boundary here would be expected to be slightly greater. Were the process to be symmetric then the number of contacts in these two scenarios should be the same; however, as the number of

contacts will be proportional to the length of the boundary between susceptible and infected and the second scenario is expected to have a larger boundary, we therefore expect a higher contact rate for  $N - k$  infected compared to  $k$  infected and, hence, a slight negative skew to the curves.

If we consider the optimal exponents found by the best fitting the  $[I(N - I)]^\alpha$  curve, across various parameter values, we can identify when the negative-quadratic of the mass-action law is appropriate, the specific parameter values for when this occurs and the parameter values for when this is not suitable. Directly considering the values of  $\alpha$  (Fig. 3), we note that as the density increases the value of  $\alpha$  tends to  $1/2$ , regardless of the straightness of the movement (value of  $\rho$ ). The value of  $\alpha$  is never greater than 0.6 except for the lowest density ( $D = 0.02$ ) with values of  $\rho > 0.6$ . That the value of  $\alpha$  never reaches 1 indicates that the mass-action law is not appropriate in these settings. Interestingly, there is a critical value of the density,  $D_c$ , at which the higher  $\rho$  valued CRW leads to fewer contacts. This is shown in Fig. 2 with the order of the curves for  $D = 0.02$  and  $D = 0.1$  going from light to dark (high to low  $\rho$ ) whereas for  $D = 0.4$  and  $D = 1$ , this has switched with curves going from dark to light (low to high  $\rho$ ). In this model, with step length fixed at 1 unit, contact distance of 2 units, and a square arena, this change is seen to occur at around  $D_c \approx 0.2$  (equivalent to  $N = 500$ ) (Supplementary Material File 3, Figure S1).

Changing the distribution of the step lengths from the fixed distance to the Rayleigh distribution does not cause any significant differences, although the Rayleigh distribution does lead to a slight increase in the contact rate (Fig. 4a1–a4, b1–b4). Comparing the best fitting values of  $\alpha$  for each distribution at each density and concentration parameter demonstrates that changing between these step length distributions does not alter the qualitative properties of the curves (Fig. 5). As expected, the uniform distribution (Fig. 4c1–c4) gives rise to curves matched

**Fig. 2** Plots showing the number of contacts between susceptible and infected as a function of the number of infected. Solid curves correspond to  $\rho = 0, 0.5, 0.7, 0.9, 0.95$  and  $0.99$  from dark to light, respectively. In all cases, the step length was fixed at 1 unit; the contact distance was fixed at  $r = 2$  units with probability of a successful contact given by  $p_{SI} = 1$ . Rows correspond to differing densities,  $D$ , of individuals relative to the area of the arena: **a, b**  $D = 0.02$  (equivalent to  $N = 50$ ); **c, d**  $D = 0.1$  ( $N = 250$ ); **e, f**  $D = 0.4$  ( $N = 1000$ ); **(g, h)**  $D = 1$  ( $N = 2500$ ). Blue dotted lines in **a, c, e, g** the first column show the best fitting negative quadratic curve; dashed lines in **b, d, f, h** the second column give the best fitting curves of the form  $(I(N - I))^\alpha$ . In all cases, the best fitting curves were determined as those that minimised the sum of the squares of the residuals between the simulated results and the fitted curve



almost perfectly by the predicted curve (dashed), regardless of value of the concentrations parameter. This predicted curve was found by calculating the percentage area of the arena expected to be covered by  $I$  disks of radius 2

(the contact distance) as discussed in the “[Analytical predictions](#)” section. It is worth noting the contact rate for the uniform distribution gives values around 10 times higher than those from the fixed or Rayleigh distribution. The

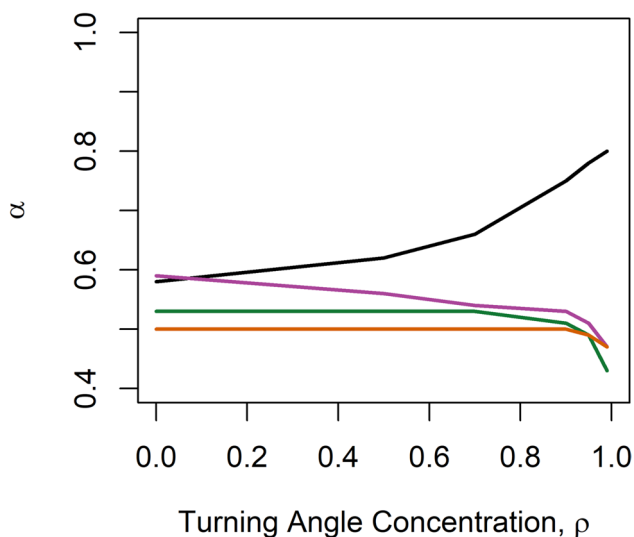


**Fig. 3** Showing the best-fitting values of  $\alpha$  against the turning angle concentration,  $\rho$ , for the curves shown in Fig. 2b, d, f, h. Colours indicate differing densities, with the following: black— $D = 0.02$ ; purple— $D = 0.1$ ; green— $D = 0.4$ ; orange— $D = 1$ . In all cases, the contact distance was  $r = 2$  and  $p_{SI} = 1$

uniform distribution also demonstrates a heavily positively skewed distribution as the density increases, although for lower densities the curves match closely to a quadratic mass-action curve (see Supplementary Material File 2 for the explanation of the positive skewness).

Considering when the rules describing a successful contact change, the results are qualitatively similar as shown by the best fit curves producing near identical values for  $\alpha$  across all concentration parameters (Fig. 6b). Figure 6a indicates the contact rate curves have been stretched by a constant, which is to be expected as these changes in rules simply reduce the number of contacts proportional to the expected value of the function for  $p_{SI}$  (see also Supplementary Material File 3, Figure S2).

Allowing the contact distance,  $r$ , to decrease but keeping the step-length the same leads to the expected decrease in the number of successful contacts for a given number of infected (Supplementary Material File 3, Fig S3-6). However, this also results in an increase in the value of  $\alpha$ , equivalent to the curves becoming more similar to the negative quadratic (Fig. 7a–c). This is most noticeable for lower densities ( $D = 0.02, 0.1$ ; black and red lines, respectively, Fig. 7); however,  $\alpha = 1$  is only approached at the extremes, that is, when movement is very straight (high  $\rho$ ) and the value of  $r$  gets small relative to the step-length. If the ratio between the step-length and contact distance is increased further ( $sl = 2$  units,  $r = 0.5$ ; Fig. 7c), this trend continues with values of  $\alpha$  seen to increase and the negative quadratic achieved ( $\alpha = 1$ ) for the lower densities, across a broader range of  $\rho$ . At high densities ( $D = 1$ ) the value of alpha remains almost constant

at  $1/2$ , indicating the best fitting curve is actually the square root of the negative quadratic.

## Discussion

Understanding how individuals interact and come into contact with each other has important implications in many fields, from ecology and epidemiology to robotics and smart cities. Here we have shown, via repeated simulation, that including a simple model for individual movement results in contact rates that can be well predicted as being proportional to  $[I(N - I)]^\alpha$  with  $\alpha \leq 1$ . Crucially, this demonstrates that the negative quadratic as assumed in many models of contact rates is only appropriate in certain cases.

In general, it was shown that the density of individuals causes a large effect on the appropriate value of  $\alpha$ , with decreasing densities having results well described by the negative quadratic of the mass-action law ( $\alpha = 1$ ), whereas increasing densities were better described by the square root of the negative quadratic ( $\alpha = 1/2$ ). The significance of the change in the value of  $\alpha$  can be seen in the qualitative difference of the predicted curves in Fig. 2, with the better-fitting curves capturing important features of the simulated results, such as significantly higher contacts for low numbers of Infected, which is important information for understanding and predicting the initial behaviour of disease and information spread. However, it should be noted that in most real-world settings the density would be expected to be lower than the smallest value considered here ( $D = 0.01$ ) and only in certain cases could these higher values be achieved; such as large crowds, peak time commuter hubs, high density farming, and large insect swarms.

Interestingly, the density of the individuals relative to the area of the arena was found to affect the movement model which gave the greatest number of contacts, with low densities requiring straighter movement, whereas higher densities required more random movement. That this change in straightness of movement affected the overall contact rate was not unexpected; however, that the density of individuals affected whether straighter or more tortuous paths gave rise to a higher contact rate was unanticipated. This could be explained by considering foraging behaviour of animals in areas of high resource value, which are characterised by highly sinuous movements (Patterson et al. 2008; Grecian et al. 2018). If we consider that at high densities individuals are constantly ‘close’ to one another and treating individuals as resources, implies that more random movements would be the most efficient. However, at low densities, we could consider the results analogous to the case for animals searching for resources. This would be similar to

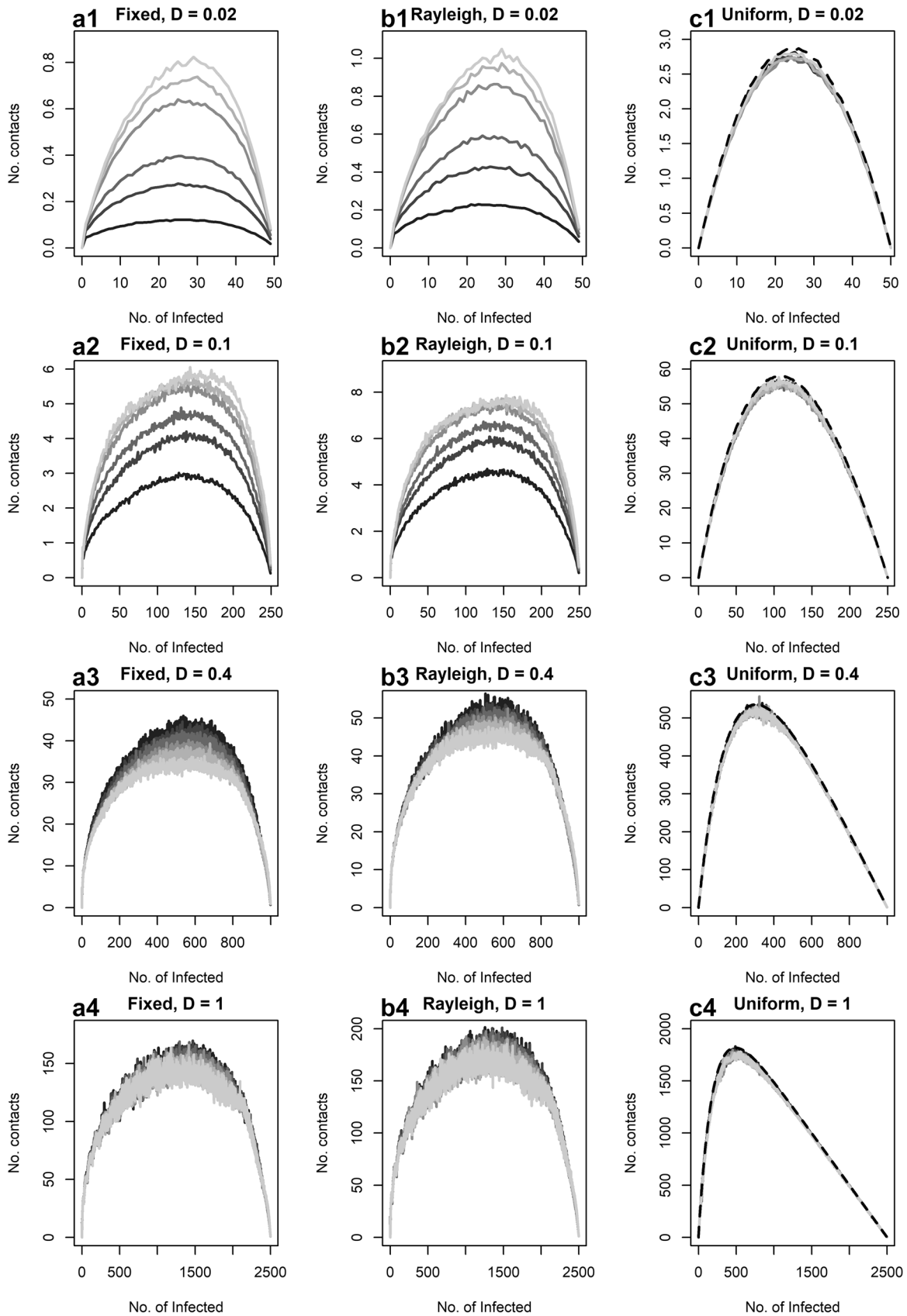




**Fig. 4** Plots comparing the effect of different step length distributions. Panels **a1–a4** used a fixed step length of 1 unit, panels **b1–b4** used a Rayleigh distribution with  $\sigma = 1$ , and panels **c1–c4** used a uniform distribution. Curves shown correspond to the concentration parameter of the wrapped normal distribution,  $\rho$ , taking values  $\rho = 0, 0.5, 0.7, 0.9, 0.95$  and  $0.99$  from dark to light, respectively. In all cases, the contact distance was fixed at  $r = 2$  units with probability of a successful contact given by  $p_{SI} = 1$ . All results are for a square arena of length 50 units. Separate rows correspond to differing densities of the number of individuals relative to the area of the arena. The dashed black line in panels **c1–c4** corresponds to the predicted curve as described in the “Analytical predictions” section

the findings of Bartumeus et al. (2005) who showed that as a simple strategy for searching, CRWs with straighter movements were more efficient. The results here indicate that  $D \sim 0.2$  is the density for which the change between straighter and more random movement occurs, although there is no clear indication for why this is the value. It also appears to have a similar value for both a fixed and Rayleigh distribution of step lengths, but this would need to be further explored in order to be generalised.

That  $\alpha$  does not tend to 1 as the density increases can be explained by noting that, at high densities, the spread of infection can be modelled as the growth of a circular wave with centre at the initial location of the original infected individual. This is because with increasing density the arena would appear homogeneous, with individuals densely and equally spread across the arena regardless of time-steps or movement model. Therefore, the infection will spread equally in all directions at each time-step, equivalent to a circular wave with a constant wavefront velocity, whereas for low densities individuals would not be densely and equally spread across the arena; therefore, the time between contacts would vary, causing the infected group to no longer grow equally in each direction and not resemble a circular wave. Assuming that the expected step length is not much larger than the contact distance, to prevent individuals from being able to ‘jump’ ahead of the wave front, then the wavefront of infection will always be ahead of the moving infected individuals and hence, the number of contacts is proportional to the increase in area that the wave covers in the next timestep. Importantly, this would not mimic the mass-action law as there is not an equal chance that at each time-step every individual is as likely to contact each other, since only individuals within the reach of the wavefront of infection will be in contact distance. This also explains why, as the density increases, the precise movement plays a less significant role in the contact dynamics (as seen in Fig. 2), as the movement does not have a large effect on the velocity of the wavefront, assuming the expected step-length is not much greater than the contact distance.

There are, however, clear limitations to these results. Notably the model for movement is discrete which assumes individuals ‘jump’ instantaneously between locations, and

therefore, the passing of information/infection can only occur at these precise locations on their movement path (although varying values for  $r$  and the distribution of step lengths were investigated to mitigate this). Therefore, a continuous movement model would be more suitable. Whilst modelling such movements are possible (Johnson et al. 2008; Michelot and Blackwell 2019), they are computationally expensive and would not be expected to greatly change the results although this could be explored. Similarly, the process treats each individual as a mass-less point particle with no physical properties to a contact or interaction; that is, movement is not affected by two individuals coming into contact nor is movement adjusted to avoid collisions. This was purely for simplicity in the model and in keeping with other similar studies (Fofana and Hurford 2017; Ahmed et al. 2021); however, more advanced individual based movement rules could be used to make this more realistic to animal movement, such as those developed for robotic group movement (Goldberg and Matarić 1999).

The movement model was strictly limited to a CRW, which is a common null model in movement and has been used in similar theoretical studies (Fofana and Hurford 2017; Ahmed and Petrovskii 2019). However, it does not usually accurately describe the complexity of movement (Fagan and Calabrese 2014). Recently, more complex models which combine both a local and long-term bias, termed biased correlated random walks (BCRW), have been developed and utilised and could be explored (Benhamou and Bovet 1992; Schultz and Crone 2001; Peleg and Mahadevan 2016; Bailey et al. 2018). Other models that have been used in similar contexts which allow for additional complexity in movement include the truncated Lévy walk (TLW) and composite correlated random walk (CCRW). TLWs assume sporadic large displacements between periods of localised Brownian motion, where the distribution of step lengths is described by a truncated power law (Rhee et al. 2011; Humphries et al. 2013), whereas in a CCRW individuals switch between CRWs with different parametrisations (Benhamou 2007; Reynolds 2014). Such behaviour has been observed in a range of organisms’ movement, including mussels (*Mytilus edulis*) (de Jager et al. 2014; Reynolds 2014) and cells (Fricke et al. 2016; Huda et al. 2018), and in humans when self-organising in crowded spaces (Murakami et al. 2019). A simple extension of this work would be to consider the effect of these more complex movement models and their effect on the expected contact rate. Hurford and Fofana (2017) did consider a truncated Lévy walk and found it was qualitatively similar to a CRW, but a deeper exploration of these other movement models should be considered.

A further development would be to incorporate and allow for individual variation within the movement model. The importance of individual variation in movement within a population is gaining importance (Delgado et al. 2018; Jolles

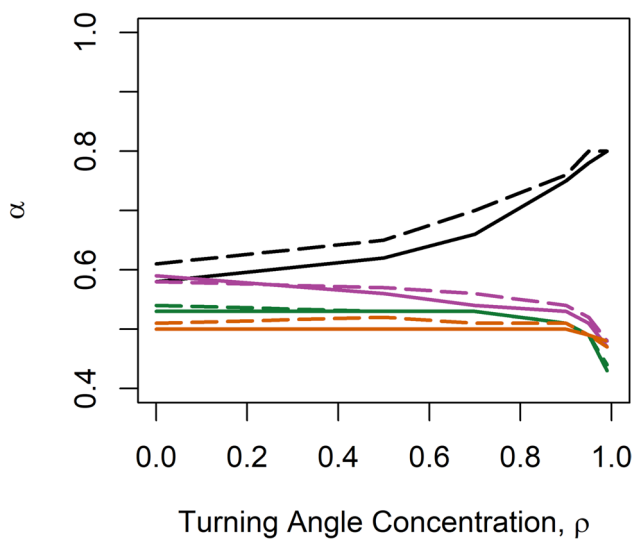


**Fig. 5** Comparing the best-fitting values of  $\alpha$  against the turning angle concentration,  $\rho$ , for different step-length distributions. Solid lines correspond to step-lengths with a fixed length of 1 unit and dashed-lines correspond to step-lengths coming from a Rayleigh distribution with  $\sigma = 1$ . Colours indicate differing densities, with: black— $D = 0.02$ ; purple— $D = 0.1$ ; green— $D = 0.4$ ; orange— $D = 1$ . In all cases the  $r = 2$

et al. 2020; Bailey et al. 2021b). Whilst variation in individual movement is usually reported when analysing movement data at the individual level, it is often averaged out at the group level with individuals' movements assumed to be from the same underlying movement model. Similarly,

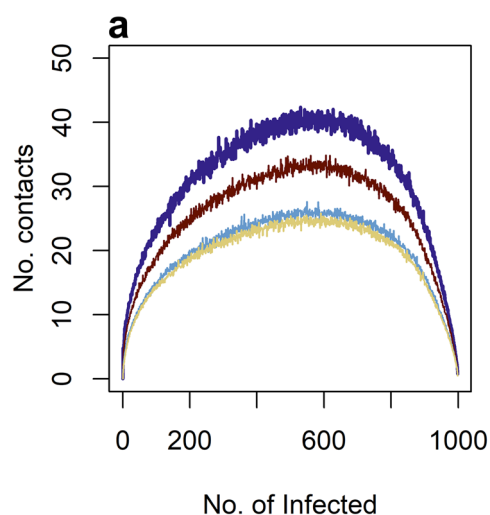
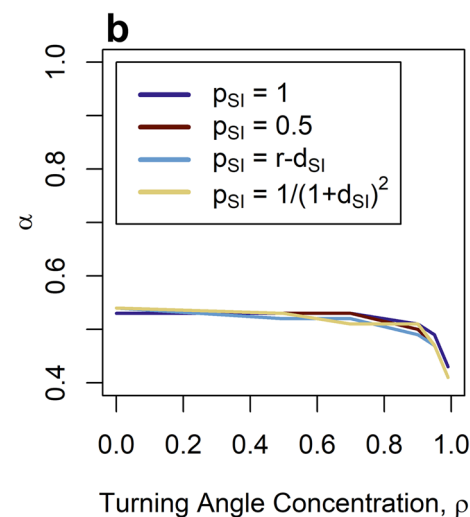


**Fig. 6** Comparing different rules for the probability of a successful contact,  $p_{SI}$ . Panel **a** shows the curves corresponding to the following rules: (i)  $p_{SI} = 1$  (purple); (ii)  $p_{SI} = 0.5$  (dark red); (iii)  $p_{SI} = r - d_{SI}$  (with  $p_{SI} = 0$  if  $d_{SI} \geq r$ ) where  $d_{SI}$  is the distance between the susceptible and infected individuals (light blue); (iv)  $p_{SI} = 1/(1 + d_{SI})^2$

many theoretical and simulation studies assume individual movement is homogeneous (Bailey et al. 2018; Ahmed and Petrovski, 2019; Pang et al. 2019). However, including greater flexibility in the parameters describing the individual level movement should increase the realism of the simulations. Similarly, throughout these simulations, the individual agents were not seen to interact with each other. In certain cases, this assumption of non-interaction may be acceptable, specifically for simpler individuals (microorganisms, insects, etc.) or in crowds where interactions are not expected to effect movement other than acting as an obstacle. However, in groups where movement can be driven by the rules of interactions (such as schools of fish, flocks of birds, and packs of mammals), then these would need to be considered. Exploring this movement would involve incorporating some group level movement models, such as those from Codling and Bode (2014), Langrock et al. (2014), Ose and Ohmann (2017), Jablonski et al. (2018), and Kay and Ohmann (2018). This could be used to explore the spread of infection/information through a large moving group of individuals, although as with the individual level, work to include individuality within these models should also be explored.

These results are indicative of simple movement in a featureless space, whereas more realistic animal movement not only involves interactions within the environment but will also depend on the drivers for an individual to move. For example, many animals display home-range behaviours, in which they move through specific areas revisiting similar locations, giving sites of high fidelity connected by common movement corridors (Powell 2000). This can be for various reasons, including



(with  $p_{SI} = 0$  if  $d_{SI} \geq r$ ) (gold). Simulations ran with the following:  $D = 0.4$  ( $N = 1000$ ),  $\rho = 0.7$ , contact distance fixed at  $r = 2$ , step-length fixed at 1 unit (results for all other values of  $\rho$  are shown in Supplementary Material File 3, Figure S2). Panel **b** displays the best fitting  $\alpha$  values for each  $p_{SI}$  rule at all  $\rho$  values

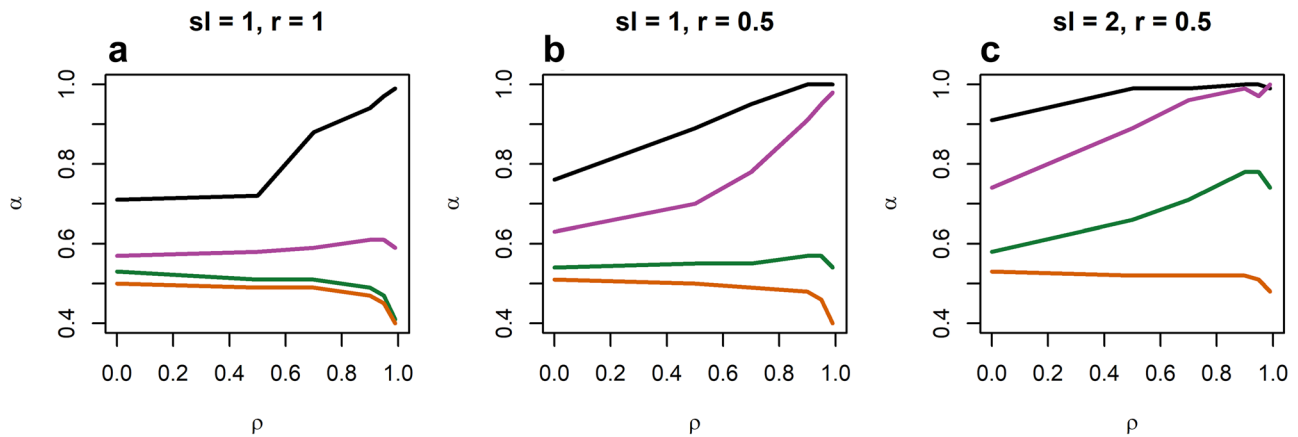


**Fig. 7** Comparing the values of  $\alpha$  for different fixed values of the step length distribution and different contact distances,  $r$ . **a** step length=1 unit,  $r = 1$ ; **b** step length=1 unit,  $r = 0.5$ ; **c** step length=2

units,  $r = 0.5$ . In all cases, curves correspond to different densities: black— $D = 0.02$ ; purple— $D = 0.1$ ; green— $D = 0.4$ ; orange— $D = 1$

patrolling, hunting/foraging, searching for mates, and defending territory (Börger and Fryxell, 2008; Powell and Mitchell 2012), and has been observed across the animal kingdom from fish (Kramer and Chapman 1999; Welsh et al. 2013) to mammals (Harris et al. 1990; Bowman et al. 2002) to birds (Ottaviani et al. 2006; Kolts and McRae 2017). In this type of movement, the contact rates between such animals would be more dependent on the crossover of these home-ranges and would depend less upon the model of movement (be it a CRW, Brownian motion, etc.). Recently, advances have been made in statistically predicting the expected number of contacts in home range movement (French et al. 2019; Martinez-Garcia et al. 2020; Ferrarini et al. 2021; Noonan et al. 2021), though these methods still rely on the acquisition of accurate telemetry data in order to inform the statistical models.

A final simple extension to this work would be to consider how and if the results are affected by incorporating some of the more complicated models used in epidemiology. For example, the SIR model allows for individuals to transition from being infected to a new state (usually labelled as recovered or removed). In this case, we would expect the results to slightly differ from those found here, as the recovered state can be thought as reducing the population size of susceptible and infected, which is equivalent to reducing their density and we would still be only interested in the contact rate between susceptible and infected. As density has been shown to have a large effect on the contact rate then we would expect this to cause a change in the results, with the transition rate from Infected to recovered being the important parameter. More complex models could also be considered, such as those that allow for reinfection, immigration/emigration, or differing levels of susceptibility.

Whilst work has been done on incorporating movement directly into models of information/disease spread (Fofana

and Hurford 2017; White et al. 2018), due to the difficulty of incorporating the displacement of even a relatively simple model of movement, such as a CRW, within the PDE framework of epidemiology, has resulted in simulations being the general approach to disease modelling when directly including movement. As stated by Fofana and Hurford (2017), incorporating these more complicated models of movement into the governing set of PDEs is an important area of research. Whilst we did not attempt the PDE approach, the results indicate that more complex movement does have an effect of the underlying assumptions of simple measures inherent in information/disease spread models and, therefore, work to fully incorporate and explore movement dynamics within the governing equations of disease/information spread is important. Such an analytical approach should also reveal the reasons behind other findings here, such as the location of the maximum number of contacts and the value for the critical density,  $D_c$ , as well as giving a more precise relationship for the number of contacts compared to the naive approximation of  $[I(N - I)]^\alpha$  used here.

**Supplementary Information** The online version contains supplementary material available at <https://doi.org/10.1007/s12080-023-00567-z>

**Author contribution** All work on the manuscript was prepared and developed by JB.

**Availability of data and material** Not applicable.

**Code availability** All code for calculating the contact rates has been uploaded as Supplementary Material File 4.

## Declarations

**Ethics approval** Not applicable.

**Consent to participate** Not applicable.

**Consent for publication** Not applicable.

**Conflicts of interest** The author declares no conflict of interests.

**Open Access** This article is licensed under a Creative Commons Attribution 4.0 International License, which permits use, sharing, adaptation, distribution and reproduction in any medium or format, as long as you give appropriate credit to the original author(s) and the source, provide a link to the Creative Commons licence, and indicate if changes were made. The images or other third party material in this article are included in the article's Creative Commons licence, unless indicated otherwise in a credit line to the material. If material is not included in the article's Creative Commons licence and your intended use is not permitted by statutory regulation or exceeds the permitted use, you will need to obtain permission directly from the copyright holder. To view a copy of this licence, visit <http://creativecommons.org/licenses/by/4.0/>.

## References

- Ahmed DA, Ansari AR, Imran M, Dingle K, Bonsall MB (2021) Mechanistic modelling of COVID-19 and the impact of lockdowns on a short-time scale. *PLoS ONE* 16(10): e0258084. <https://doi.org/10.1371/journal.pone.0258084>
- Ahmed DA, Petrovskii SV (2019) Analysing the impact of trap shape and movement behaviour of ground-dwelling arthropods on trap efficiency. *Methods Ecol Evol* 10:1246–1264
- Allema AB, Rossing WAH, van der Werf W, Volker D, Marsan D, Steingröver EG, van Lenteren JC (2010) Ground beetle dispersal: how to bridge the scales? In IOBC/WPRS Working Group Landscape Management for Functional Biodiversity, Cambridge, UK 56:5–8
- Andersen MC, Ewald M, Northcott J (2005) Risk analysis and management decisions for weed biological control agents: ecological theory and modeling results. *Biol Control* 35(3):330–337
- Bailey JD, Benefer CM, Blackshaw RP, Codling EA (2021a) Walking behaviour in the ground beetle, *Poecilus cupreus*: dispersal potential, intermittency and individual variation. *Bull Entomol Res* 111(2):200–209
- Bailey JD, Codling EA (2021) Emergence of the wrapped Cauchy distribution in mixed directional data. *ASTA Adv Stat Anal* 105:229–246
- Bailey JD, King AJ, Codling EA, Short AM, Johns GI, Fürtbauer I (2021b) “Micropersonality” traits and their implications for behavioral and movement ecology research. *Ecol Evol* 11:3264–3273
- Bailey JD, Wallis J, Codling EA (2018) Navigational efficiency in a biased and correlated random walk model of individual animal movement. *Ecology* 99(1):217–223
- Banks JE, Laubmeier AN, Banks HT (2020) Modelling the effects of field spatial scale and natural enemy colonization behaviour on pest suppression in diversified agroecosystems. *Agric Forest Entomol* 22:30–40
- Bansal S, Grenfell BT, Meyers LA (2007) When individual behaviour matters: homogeneous and network models in epidemiology. *J Royal Soc Interf* 4(16):879–891
- Bansal S, Read J, Pourbohloul B, Meyers LA (2010) The dynamic nature of contact networks in infectious disease epidemiology. *J Biol Dyn* 4(5):478–489
- Bartumeus F, Catalan J, Viswanathan G, Raposo E, Da Luz M (2008) The influence of turning angles on the success of non-oriented animal searches. *J Theor Biol* 252:43–55
- Bartumeus F, da Luz MGE, Viswanathan GM, Catalan J (2005) Animal search strategies: a quantitative random-walk analysis. *Ecology* 86(11):3078–3087
- Bartumeus F, Giuggioli L, Louzao M, Bretagnolle V, Oro D, Levin SA (2010) Fishery discards impact on seabird movement patterns at regional scales. *Curr Biol* 20(3):215–222
- Bau J, Cardé RT (2016) Simulation modeling to interpret the captures of moths in pheromone-baited traps used for surveillance of invasive species: the gypsy moth as a model case. *J Chem Ecol* 42:877–887
- Bearup D, Petrovskii S (2015) On time scale invariance of random walks in confined space. *J Theor Biol* 367:230–245
- Bearup D, Benefer CM, Petrovskii SV, Blackshaw RP (2016) Revisiting Brownian motion as a description of animal movement: a comparison to experimental movement data. *Methods Ecol Evol* 7(12):1525–1537
- Benhamou S (2006) Detecting an orientation component in animal paths when the preferred direction is individual-dependent. *Ecology* 87(2):518–528
- Benhamou S (2007) How many animals really do the Lévy walk. *Ecology* 88:518–528
- Benhamou S, Bovet P (1992) Distinguishing between elementary orientation mechanisms by means of path analysis. *Anim Behav* 43(3):371–377
- Bergman CM, Schaefer JA, Lutich SN (2000) Caribou movement as a correlated random walk. *Oecologia* 123(3):364–374
- Blackwell PG (1997) Random diffusion models for animal movement. *Ecol Model* 100(1–3):87–102
- Börger L, Dalziel BD, Fryxell JM (2008) Are there general mechanisms of animal home range behaviour? A review and prospects for future research. *Ecol Lett* 11:637–650
- Bowman J, Jaeger JA, Fahrig L (2002) Dispersal distance of mammals is proportional to home range size. *Ecology* 83(7):2049–2055
- Byers JA (2001) Correlated random walk equations of animal dispersal resolved by simulation. *Ecology* 79(6):1680–1690
- Byers JA (2009) Modeling distributions of flying insects: effective attraction radius of pheromone in two and three dimensions. *J Theor Biol* 256:81–89
- Byers JA, Naranjo SE (2014) Detection and monitoring of pink bollworm moths and invasive insects using pheromone traps and encounter rate models. *J Appl Ecol* 51(4):1041–1049
- Christensen K, Cocconi L, Sendova-Franks AB (2021) Animal intermittent locomotion: a null model for the probability of moving forward in bounded space. *J Theor Biol* 510:110533
- Codling EA, Bearon RN, Thorn GJ (2010) Diffusion about the mean drift location in a biased random walk. *Ecology* 91:3106–3113
- Codling EA, Bode NW (2014) Copycat dynamics in leaderless animal group navigation. *Move Ecol* 2(1):1–11
- Codling EA, Plank MJ, Benhamou S (2008) Random walks in biology. *J Royal Soc Interf* 5:813–834
- de Jager M, Bartumeus F, Kölzsch A, Weissing FJ, Hengeveld GM, Nolet BA, Herman PMJ, Van de Koppel J (2014) How superdiffusion gets arrested: ecological encounters explain shift from Lévy to Brownian movement. *Proceedings of the Royal Society b: Biological Sciences* 281(1774):20132605
- Delgado MDM, Miranda M, Alvarez SJ, Gurarie E, Fagan WF, Penteriani V, di Virgilio A, Morales JM (2018) The importance of individual variation in the dynamics of animal collective movements. *Philos Transact Royal Soc b: Biol Sci* 373(1746):20170008
- Dimidov C, Oriolo G, and Trianni V (2016) Random walks in swarm robotics: an experiment with kilobots. *Int Conf Swarm Intell* 185–196. Springer, Cham
- Dougherty ER, Seidel DP, Carlson CJ, Spiegel O, Getz WM (2018) Going through the motions: incorporating movement analyses into disease research. *Ecol Lett* 21(4):588–604
- Fagan WF, Calabrese JM (2014) The correlated random walk and the rise of movement ecology. *Bull Ecol Soc Am* 95:204–206
- Ferrarini A, Giglio G, Pellegrino SC, Gustin M (2021) A new general index of home range overlap and segregation: the Lesser Kestrel in Southern Italy as a case study. *Avian Res* 12:4

- Focardi S, Cecere JG (2014) The Lévy flight foraging hypothesis in a pelagic seabird. *J Animal Ecol* 83(2):353–364
- Fofana AM, Hurford A (2017) Mechanistic movement models to understand epidemic spread. *Philos Transact Royal Soc b: Biol Sci* 372(1719):20160086
- Fortin D, Beyer HL, Boyce MS, Smith DW, Duchesne T, Mao JS (2005) Wolves influence elk movements: behavior shapes a trophic cascade in Yellowstone National Park. *Ecology* 86(5):1320–1330
- Franz B, Erban R (2013) Hybrid modelling of individual movement and collective behaviour. *Dispersal, individual movement and spatial ecology*. Springer, Berlin, Heidelberg, pp 129–157
- French JT, Wang HH, Grant WE, Tomeček JM (2019) Dynamics of animal joint space use: a novel application of a time series approach. *Move Ecol* 7:38
- Fricke GM, Letendre KA, Moses ME, Cannon JL (2016) Persistence and adaptation in immunity: T cells balance the extent and thoroughness of search. *PLoS Comput Biol* 12:e1004818
- Garcia M, Berti S, Peyla P, Rafai S (2011) Random walk of a swimmer in a low-Reynolds-number medium. *Phys Rev E* 83(3):035301
- Goldberg D, and Mataric MJ (1999) Coordinating mobile robot group behavior using a model of interaction dynamics. In *Proceedings of the third annual conference on Autonomous Agents* 100–107
- Grant TJ, Parry HR, Zalucki MP, Bradbury SP (2018) Predicting monarch butterfly (*Danaus plexippus*) movement and egg-laying with a spatially-explicit agent-based model: the role of monarch perceptual range and spatial memory. *Ecol Model* 374:37–50
- Grecian WJ, Lane JV, Michelot T, Wade HM, Hamer KC (2018) Understanding the ontogeny of foraging behaviour: insights from combining marine predator bio-logging with satellite-derived oceanography in hidden Markov models. *J Royal Soc Interf* 15(143):20180084
- Gui LY, Boiteau G, Colpitts BG, MacKinley P, McCarthy PC (2012) Random movement pattern of fed and unfed adult Colorado potato beetles in bare-ground habitat. *Agric Forest Entomol* 14(1):59–68
- Hall PG (1988) *Introduction to the theory of coverage processes*. John Wiley & Sons, New York
- Harris S, Cresswell WJ, Forde PG, Trehwella WJ, Woollard T, Wray S (1990) Home-range analysis using radio-tracking data—a review of problems and techniques particularly as applied to the study of mammals. *Mammal Rev* 20(2–3):97–123
- Haydon DT, Morales JM, Yott A, Jenkins DA, Rosatte R, Fryxell JM (2008) Socially informed random walks: incorporating group dynamics into models of population spread and growth. *Proceedings Biol Sci* 275(1638):1101–1109
- Horne JS, Garton EO, Krone SM, Lewis JS (2007) Analyzing animal movements using Brownian bridges. *Ecology* 88(9):2354–2363
- Huang ZF (2000) Self-organized model for information spread in financial markets. *Eur Phys J B-Condens Matter Complex Syst* 16(2):379–385
- Huda S, Weigelin B, Wolf K et al (2018) Lévy-like movement patterns of metastatic cancer cells revealed in microfabricated systems and implicated in vivo. *Nature Commun* 9(1):1–11
- Hudson EG, Brookes VJ, Ward MP, and Dürr S (2019) Using roaming behaviours of dogs to estimate contact rates: the predicted effect on rabies spread. *Epidemiol Infect* 147
- Humphries NE, Weimerskirch H, Sims DW (2013) A new approach for objective identification of turns and steps in organism movement data relevant to random walk modelling. *Methods Ecol Evol* 4(10):930–938
- Jablonski KE, Boone RB, Meiman PJ (2018) An agent-based model of cattle grazing toxic Geyer's larkspur. *PLoS ONE* 13(3):e0194450
- Jiao W, Gonella S (2020) Dynamics of interacting particle systems: Modeling implications of the repulsive interactions and experiments on magnetic prototypes. *Phys Rev B* 102(5):054304
- Johnson DS, London JM, Lea MA, Durban JW (2008) Continuous-time correlated random walk model for animal telemetry data. *Ecology* 89(5):1208–1215
- Jolles JW, King AJ, Killen SS (2020) The role of individual heterogeneity in collective animal behaviour. *Trends Ecol Evol* 35(3):278–291
- Kareiva PM, Shigesada N (1983) Analyzing insect movement as a correlated random walk. *Oecologia* 56(2–3):234–238
- Kay TM, Ohmann PR (2018) Effects of random motion in traveling and grazing herds. *J Theor Biol* 456:168–174
- Kegeleirs M, Ramos DG, and Birattari M (2019) Random walk exploration for swarm mapping. *Annl Conf Towards Auton Rob Syst* 211–222. Springer, Cham
- Kirkeby C, Halasa T, Gussmann M, Toft N, Græsbøll K (2017) Methods for estimating disease transmission rates: evaluating the precision of Poisson regression and two novel methods. *Sci Rep* 7(1):1–11
- Koh I, Rowe HI, Holland JD (2013) Graph and circuit theory connectivity models of conservation biological control agents. *Ecol Appl* 23(7):1554–1573
- Kolts JR, McRae SB (2017) Seasonal home range dynamics and sex differences in habitat use in a threatened, coastal marsh bird. *Ecol Evol* 7(4):1101–1111
- Kramer DL, Chapman MR (1999) Implications of fish home range size and relocation for marine reserve function. *Environ Biol Fishes* 55(1):65–79
- Langrock R, Hopcraft JGC, Blackwell PG, Goodall V, King R, Niu M, Patterson TA, Pedersen MW, Skarin A, Schick RS (2014) Modelling group dynamic animal movement. *Methods Ecol Evol* 5(2):190–199
- Li L, Wang BH, Wang S, Moalim-Nour L, Mohib K, Lohnes D, Wang L (2010) Individual cell movement, asymmetric colony expansion, rho-associated kinase, and E-cadherin impact the clonogenicity of human embryonic stem cells. *Biophys J* 98(11):2442–2451
- Liggett TM (2012) *Interacting particle systems* 276. Springer Science & Business Media. Springer, New York
- Loureiro AM, Nams VO (2020) Sand and shine: an inexpensive method to measure terrestrial arthropod movement in the laboratory. *Can Entomol* 152(6):823–829
- Manoukis N, Hall B, Geib S (2014) A computer model of insect traps in a landscape. *Sci Rep* 4(1):1–8
- Martinez-Garcia R, Fleming CH, Seppelt R, Fagan WF, Calabrese JM (2020) How range residency and long-range perception change encounter rates. *J Theor Biol* 498:110267
- McDermott PL, Wikle CK, Millspaugh J (2017) Hierarchical nonlinear spatio-temporal agent-based models for collective animal movement. *J Agric Biol Environ Stat* 22(3):294–312
- Menden-Deuer S (2010) Inherent high correlation of individual motility enhances population dispersal in a heterotrophic, planktonic protist. *PLoS Comput Biol* 6(10):e1000942
- Michelot T, Blackwell PG (2019) State-switching continuous-time correlated random walks. *Methods Ecol Evol* 10(5):637–649
- Murakami H, Feliciani C, Nishinari K (2019) Lévy walk process in self-organization of pedestrian crowds. *J R Soc Interface* 16(153):20180939
- Nathan R, Getz WM, Revilla E, Holyoak M, Kadmon R, Saltz D, Smouse PE (2008) A movement ecology paradigm for unifying organismal movement research. *Proc Natl Acad Sci* 105(49):19052–19059
- Noonan MJ, Martinez-Garcia R, Davis GH, Crofoot MC, Kays R, Hirsch BT, Caillaud D, Payne E, Sih A, Sinn DL, Spiegel O, Fagan WF, Fleming CH, Calabrese JM (2021) Estimating encounter location distributions from animal tracking data. *Methods Ecol Evol* 12(7):1158–1173
- Ose NJ, Ohmann PR (2017) The selfish herd: noise effects in local crowded horizon and voronoi models. *J Theor Biol* 424:84–90

- Ottaviani D, Cairns SC, Oliverio M, Boitani L (2006) Body mass as a predictive variable of home-range size among Italian mammals and birds. *J Zool* 269(3):317–330
- Otten W, Filipe JAN, Bailey DJ, Gilligan CA (2003) Quantification and analysis of transmission rates for soilborne epidemics. *Ecology* 84(12):3232–3239
- Ovaskainen O (2004) Habitat-specific movement parameters estimated using mark-recapture data and a diffusion model. *Ecology* 85:242–257
- Pang B, Qi J, Zhang C, Song Y, and Yang R (2019) Analysis of random walk models in swarm robots for area exploration. *IEEE Int Conf Rob Biomimet* 2484–2489. IEEE
- Pang B, Song Y, Zhang C, and Yang R (2021) Effect of random walk methods on searching efficiency in swarm robots for area exploration. *Appl Intell* 1–11
- Papastamatiou YP, DeSalles PA, McCauley DJ (2012) Area-restricted searching by manta rays and their response to spatial scale in lagoon habitats. *Mar Ecol Prog Ser* 456:233–244
- Patterson TA, Thomas L, Wilcox C, Ovaskainen O, Matthiopoulos J (2008) State–space models of individual animal movement. *Trends Ecol Evol* 23(2):87–94
- Peleg O, Mahadevan L (2016) Optimal switching between geocentric and egocentric strategies in navigation. *Royal Soc Open Sci* 3(7):160128
- Powell RA (2000) Animal home ranges and territories and home range estimators. In: Boitani L, Fuller TK (eds) *Research techniques in animal ecology: controversies and consequences*. Columbia University Press, New York, New York, USA, pp 65–110
- Powell RA, Mitchell MS (2012) What is a home range? *J Mammal* 93(4):14
- R Core Team (2020) *A language and environment for statistical computing*. R Foundation for Statistical Computing, Vienna, Austria. URL <https://www.R-project.org/>
- Renzaglia A, Briñón-Arranz L (2020) Search and localization of a weak source with a multi-robot formation. *J Intell Rob Syst* 97(3):623–634
- Reynolds AM (2014) Mussels realize Weierstrassian Lévy walks as composite correlated random walks. *Sci Rep* 4(1):1–5
- Reynolds AM, Leprêtre L, Bohan DA (2013) Movement patterns of *Tenebrio* beetles demonstrate empirically that correlated-random-walks have similitude with a Lévy walk. *Sci Rep* 3(1):1–8
- Rhee I, Shin M, Hong S, Lee K, Kim SJ, Chong S (2011) On the levy-walk nature of human mobility. *IEEE/ACM Trans Networking* 19(3):630–643
- Richomme C, Gauthier D, Fromont E (2006) Contact rates and exposure to inter-species disease transmission in mountain ungulates. *Epidemiol Infect* 134(1):21–30
- Schultz CB, Crone EE (2001) Edge-mediated dispersal behavior in a prairie butterfly. *Ecology* 82(7):1879–1892
- Tang W, Bennett DA (2010) Agent-based modeling of animal movement: a review. *Geogr Compass* 4(7):682–700
- Theves M, Taktikos J, Zaburdaev V, Stark H, Beta C (2015) Random walk patterns of a soil bacterium in open and confined environments. *EPL (europhysics Letters)* 109(2):28007
- Tracey JA, Bevins SN, VandeWoude S, Crooks KR (2014) An agent-based movement model to assess the impact of landscape fragmentation on disease transmission. *Ecosphere* 5(9):1–24
- Turchin P (1998) *Quantitative analysis of movement: measuring and modeling population redistribution in animals and plants*. Sinauer Associates, Sunderland, Massachusetts, USA
- Volkova VV, Howey R, Savill NJ, Woolhouse ME (2010) Sheep movement networks and the transmission of infectious diseases. *PLoS ONE* 5(6):e11185
- Welsh JQ, Goatley CHR, Bellwood DR (2013) The ontogeny of home ranges: evidence from coral reef fishes. *Proc Royal Soc b: Biol Sci* 280(1773):20132066
- White LA, Forester JD, Craft ME (2018) Dynamic, spatial models of parasite transmission in wildlife: their structure, applications and remaining challenges. *J Anim Ecol* 87(3):559–580
- Whitehead H, Coakes A, Jaquet N, Lusseau S (2008) Movements of sperm whales in the tropical Pacific. *Mar Ecol Prog Ser* 361:291–300
- Wittman JT, Nicoll RA, Myers SW, Chaloux PH, Aukema BH (2019) Characterizing and simulating the movement of late-instar gypsy moth (*Lepidoptera: Erebidae*) to evaluate the effectiveness of regulatory practices. *Environ Entomol* 48(3):496–505
- Zhou B, Pei S, Muchnik L, Meng X, Xu X, Sela A, Havlin S, Stanley HE (2020) Realistic modelling of information spread using peer-to-peer diffusion patterns. *Nat Hum Behav* 4(11):1198–1207